Int. J. Electrochem. Sci., 15 **(2020)** 2089 – 2100, doi: 10.20964/2020.03.67

International Journal of
ELECTROCHEMICAL
SCIENCE
www.electrochemsci.org

Combined Effect of Cathodic Potential and Heat Treatment on Stress Corrosion Cracking Behaviour of Low Alloy Steel in Artificial Seawater

Daixun Jiang[1], *Jiangfeng An* [2,3], *Jun Wu*[2,3,*], *Penghua Zheng*[2,3]

[1] CRRC Qingdao Sifang Co. Ltd, No.88 Jinhongdong Road, Qingdao, 266111, China
[2] Wuhan Research Institute of Materials Protection Co., Ltd, 126 Bao Feng Erlu, Wuhan, Hubei 430030, China
[3] Wuhan Materials Corrosion of Atmospheric Environment National Observation and Research Station, 6 Jin Tan lu, Wuhan, Hubei 430030, China
[*]E-mail: cbswuj@sina.com

Received: 4 November 2019 / *Accepted:* 12 January 2020 / *Published:* 10 February 2020

In this study, the SCC behaviour and mechanism of E690 steels with different heat treatments were investigated in artificial seawater by slow strain rate test, surface analysis technique and potentiodynamic polarization curve test. The results show that the SCC behaviour of E690 steel is mainly controlled by anodic dissolution, and the steels after tempering show the high SCC susceptibilities because of the high corrosion current densities. As the cathodic potential negatively decreases to -850 mV, the SCC susceptibility of base metal decreases; however, the SCC susceptibilities of the steels after tempering increase. At -1050 mV, the SCC susceptibilities of the steels with different heat treatments increase. And the SCC susceptibilities of the steels after tempering are higher than those of base metal at various potentials. The phenomenon is related to the high hydrogen embrittlement susceptibilities of the steels after tempering compared to that of the base metal.

Keywords: Low alloy steel; Heat treatment; Cathodic potential; Stress corrosion cracking

1. INTRODUCTION

The stress corrosion cracking (SCC) was considered as one of main reasons for the fracture failure of ocean engineering equipment [1]. Many measures have been investigated to slow the corrosion of metals, such as using protective coatings or providing cathodic protection [2-8]. The previous studies have shown that an applied cathodic potential impacted the corrosion behaviour, especially SCC behaviour [7-9]. Many studies have demonstrated that there is an optimal cathodic protection potential for restraining SCC [5, 7, 8]. And, the SCC behaviour and mechanism were

influenced by environment, organization structure and constituents of metal, which affected the value of optimal cathodic potential [10-16]. The wrong applied potential even enhances SCC susceptibility [5, 7-9]. Thus, it is necessary to investigate the SCC behaviour and mechanism.

The SCC behaviour of low alloy steel was generally considered to be controlled by anodic dissolution and hydrogen embrittlement (HE) [5, 8], which was determined by pH value in the environment [17-22]. In high pH environment, such as a concentrated carbonate/bicarbonate environment, SCC usually occurs in an intergranular cracking [18]. It has been demonstrated that SCC in high pH environment was related to anodic dissolution at the grain boundaries and repeated rupture of passive films that form over the crack tip [23]. In a near-neutral pH environment, SCC of low alloy steel usually occurs with a transgranular, quasi-cleavage crack morphology with very little branching, such as SCC in the electrolyte environment characterized with anaerobic, dilute solutions with a pH in the range of 6–7.5. It has been accepted that the above SCC behaviour was associated with anodic dissolution and the permeation of hydrogen atoms into the steel. The previous work has pointed out that the hydrogen atoms in the metal would accelerate anodic dissolution in bicarbonate solution, resulted from the alteration of chemical potential of steel upon hydrogen-charging [24]. And, it was indicated that hydrogen on the surface of the steel could diffuse into the specimen around the crack tip during. And hydrogen in the metal enhanced the electrochemical reaction rate, which would lead to an increase of SCC susceptibility [9, 20]. Zhao et al. demonstrated that the SCC behaviour was controlled by the interaction of the hydrogen, stress, anodic dislocation [25, 26] . It was illustrated that the concentrate of hydrogen and anodic dissolution depended on the pH value and applied potential [7, 22, 27-29].With negative decrease of applied cathodic potential, anodic dissolution was inhibited and hydrogen evolution reaction was enhanced, both of which controlled SCC mechanism [28].The inhibition of anodic dissolution has a favorable effect on the decrease of SCC susceptibility [7, 30]. When the accumulation of hydrogen atoms exceed a certain value, the negative decrease of applied cathodic potential would accelerate SCC susceptibility [9]. At the relatively negative cathodic potential, the negatively decrease of cathodic potential accelerated HE susceptibility, resulting in a higher SCC susceptibility [8].

On the other hand, the variation in the steel microstructure impacts the SCC behaviour [5, 31-34]. In actual ocean engineering, the welding joint is essential in large engineering equipment. The microstructures in the heat-affected zone are varied because of the different peak weld temperatures and the distances from the welding line during the welding process [35, 36]. It has been shown that the SCC behaviour is impacted by microstructure variations [10-12]. The corrosion rates of ferrite, pearlite, austenite and lath martensite gradually increase in a NaCl solution with a pH value of 6.0 [13, 14]. Bulger et al. further pointed out that the SCC susceptibility of ferritic–pearlitic microstructures is higher than that of bainitic–ferritic microstructures in near-neutral pH environments [15]. It was concluded that the HE susceptibilities of the welded joints in high-strength steels are higher than those of the corresponding basic metal in a seawater environment [16]. It was considered that the strain-hardening-induced local deformation within the welding joint of high-strength steel is the main reason for the high SCC susceptibility [37]. Thus, it can be concluded that the variation of microstructures within the welding joint will influence the SCC behaviour, further resulting in altering the value of the optimal cathodic potential. It is essential to study the effect of microstructure variations on SCC

behaviour under a cathodic potential, which is related to the welding process.

In this work, the SCC behaviours of E690 steel with different heat treatments are studied under a cathodic potential in artificial seawater with slow strain rate tensile tests (SSRTs), surface analysis techniques, and electrochemical measurements. The hope is that this research can provide a critical reference for correctly applying cathodic potentials and controlling SCC in welding joints of high-strength steel.

2. EXPERIMENTAL

In this work, a low-alloy steel, E690 steel, was used from a Chinese steel company with the following chemical composition (wt.%): 0.15% C, 1.00% Mn, 0.0058% P, 0.0014% S, 0.99% Cr, 0.20% Si, 1.45% Ni, 0.37% Mo, 0.036% Al, 0.033% V and a balance of Fe. To perform heat treatments, E690 steel plates were cut into samples with dimensions of 15 × 20 × 145 mm and then kept in a furnace at 960 °C for 12 min. Finally, the heat-treated specimens were cooled in water and a furnace, with cooling rates of 200~400 °C/s and 1~3 °C/s, respectively.

All experiments were conducted in artificial seawater based on ASTM D1141, with the composition shown in Table 1. The pH value of the artificial seawater was adjusted to 8.1 by 0.1 mol/L HCl and NaOH solutions.

Table 1. Main components of the artificial seawater in g/L (ASTM D1141)

NaCl	$MgCl_2$	Na_2SO_4	$CaCl_2$	KCl	$NaHCO_3$	H_3BO_3	$SrCl_2$	NaF
24.53	5.2	4.09	1.16	0.695	0.201	0.027	0.025	0.003

Samples with dimensions of 10 × 10 × 2 mm were cut from the heat-treated plates and the E690 basic metal plate. The samples were gradually ground to a 1500 grit by emery paper, and then they were polished with a diamond suspension abrasive until there were no scratches. The samples were etched with a 4 wt.% Nital solution, cleaned with deionized water, and then dried in air. Subsequently, the microstructures were observed by an optical microscope.

The SCC behaviours of the heat-treated and E690 basic metal were investigated by SSRT. The specimens for SSRT were cut according to the GB T15970 specification. The test section was polished sequentially to 1500 grit with emery paper, and the other parts were sealed by silica gel. A traditional three-electrode system was used to apply a cathodic potential, with an SSRT specimen, a platinum sheet and a saturated calomel electrode (SCE) working as the working electrode, counter electrode and reference electrode, respectively. Prior to the test, the samples were immersed in the solution for 24 h under a cathodic potential. Then, the tests were conducted both in air and in solution under various potentials, with a tensile rate of 0.0018 mm/min, and a strain rate of 1×10^{-6} s^{-1}, by using a WDML-

30KN Materials Test System (made in China). After failure of the specimens, the cross-sectional area of the fracture and the extended length of the specimen were measured. The loss percentage of area reduction (I_Ψ) and the elongation (I_δ) were calculated with the following expressions to evaluate the SCC susceptibilities at various potentials:

$$I_\Psi = \left(1 - \frac{\Psi_S}{\Psi_0}\right) \times 100\% \quad (1)$$

$$I_\delta = \left(1 - \frac{\delta_S}{\delta_0}\right) \times 100\% \quad (2)$$

where Ψ_0 and Ψ_s are the area reduction measured in air and artificial seawater, respectively, and δ_0 and δ_s are the elongation in air and artificial seawater, respectively. After that, the fractures were cut from the specimens to derust with a rust remover (500 ml HCl, 500 ml deionized water, 6 g hexamethylene tetramine), and then, the fracture surfaces and side faces were observed by scanning electron microscopy (SEM, Cambridge S-360 SEM) to determine the rupture sensitivity.

During the electrochemical tests, the heat treatment and base metal samples with dimensions of 10 × 10 × 2 mm were used as the working electrode. The samples were embedded in epoxy resin after welding with copper wires, leaving a working area of 10 ×10 mm. The working surface was grounded to 1500 grit with emery paper, cleaned with alcohol, and then dried in air. Potentiodynamic polarization curves were measured in artificial seawater through a electrochemical workstation using a three-electrode system, with the platinum sheet and saturated calomel electrode as counter electrode and reference electrode, respectively. The polarization curves were performed within the scanning range from –950 mV to -200 mV (vs. SCE) at scanning rates of 0.5 mV/s.

All the measurements were repeated at least three times to ensure the reproducibility and reliability of the results at a room temperature of 25 ± 1 ºC. All the potentials shown in this paper are with reference to the SCE.

3. RESULTS AND DISCUSSIONS

3.1 Microstructures of E690 steel specimen

Fig. 1 shows the microstructure of the basic metal and the microstructures under the different heat treatments. It can be observed that the approximately parallel ferrite laths are distributed in the former austenite grains in Fig. 1a. Fig. 1b shows that martensite and pearlite appear among the lath bainite. This may be caused by the accumulation of carbon atoms during tempering. Fig. 1c shows a ferrite matrix with a few small, dark martensite-austenitic particles at grain boundaries, which is related to the rapid cooling rate.

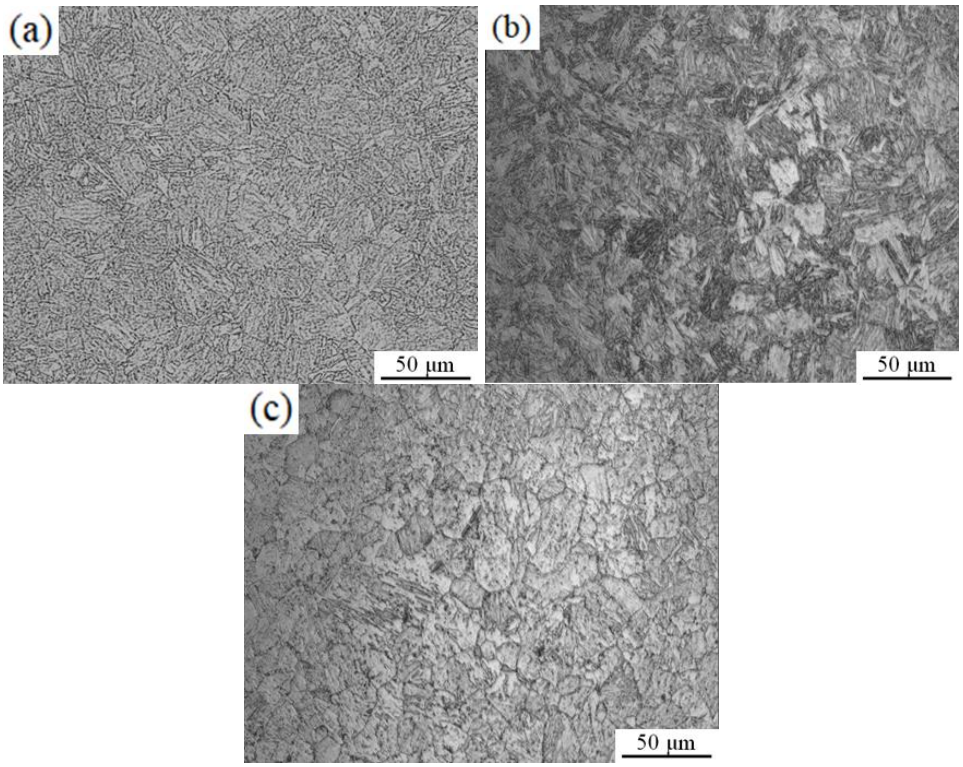

Figure 1. Microstructures of E690 steel with the different heat treatments: (a) base metal; (b) cooling in a furnace; and (c) cooling in water

3.2. Slow strain rate tensile tests

Fig. 2 shows the SSRT curves and the corresponding susceptibility of E690 steel with the different heat treatments under various potentials in artificial seawater. No obvious yield strength points appear on the stress-strain curves of the microstructures with heat treatment, and only the basic metal exhibits an obvious yield strength point. The Young's modulus values for the three microstructures is different. It is indicated that the physical characteristics of the metal are influenced by the variation in the microstructures, which is related to the heat treatment method. The tensile strength of the metal after heat treatment is higher than that of the basic metal, and the tensile strength of the sample cooled in water shows the highest tensile strength, which is considered to be caused by the residual stress efficiently distributing in the metal from the rapid cooling rate.

For all three heat treatments, the stress-strain curves in air show the highest elongation. This means that steels with different heat treatments under various potentials exhibit a certain SCC susceptibility. Thus, I_Ψ and I_δ were calculated, with the results shown in Fig. $2a_2$, b_2 and c_2. The microstructures of the three different heat treatments exhibit different variations in I_Ψ and I_δ, with the applied potential decreasing from the open circuit potential (OCP) to -1050 mV. Both I_Ψ and I_δ of the basic metal decrease first and then increase with a negative shift of potential, and the lowest values occur at -850 mV. However, both I_Ψ and I_δ of the steels with different cooling rates gradually increase as the applied potential decreases.

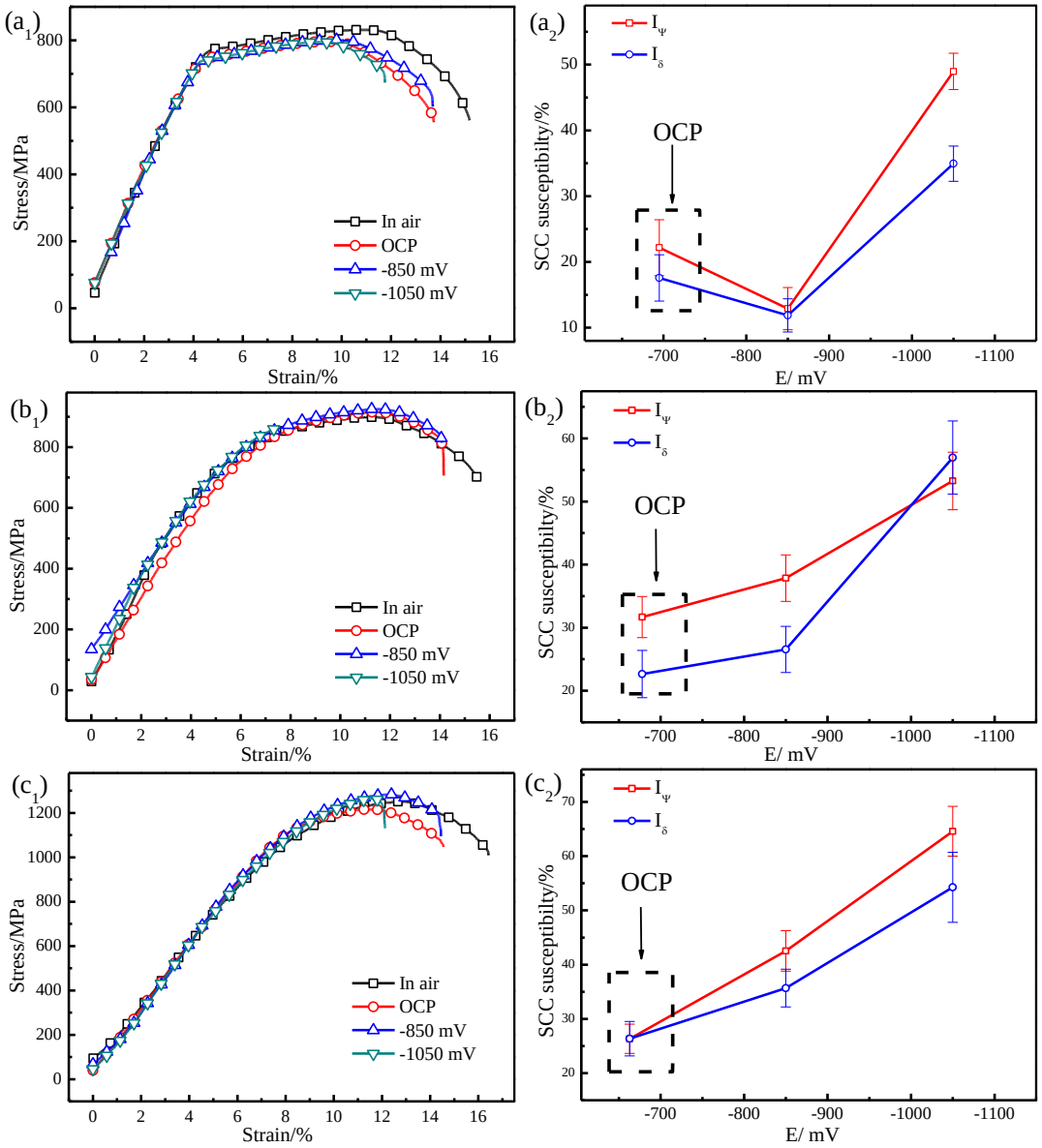

Figure 2. Stress-strain curves (a_1, b_1, c_1) and corresponding susceptibility (a_2, b_2, c_2) of E690 steel with the different heat treatments under various potentials in artificial seawater: (a_1, a_2) base metal; (b_1, b_2) cooling in a furnace; and (c_1, c_2) cooling in water

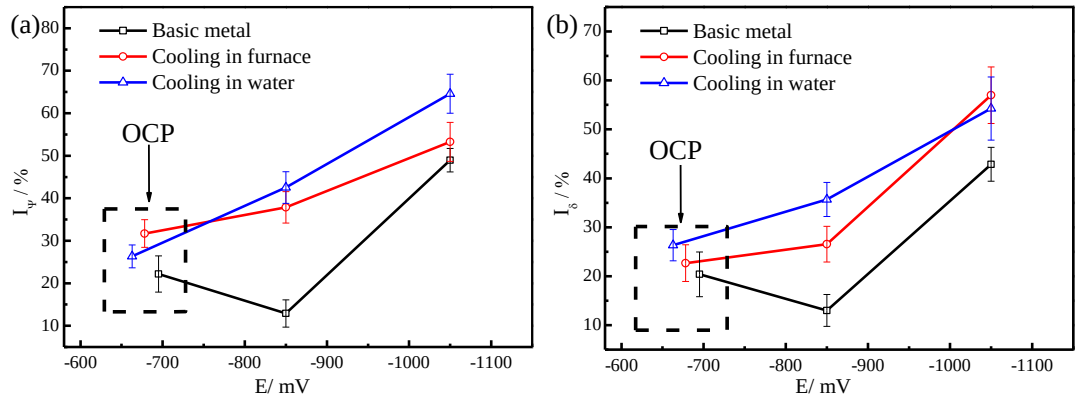

Figure 3. SCC susceptibility of E690 steels with the different heat treatments: (a) the loss rate of area reduction and (b) the loss rate of elongation

To further analyse the effect of heat treatments on SCC susceptibility, the values of the SCC susceptibilities with different heat treatments were compared, with the results shown in Fig. 3. In Figs. 3a and b, the base metal exhibits the lowest I_Ψ and I_δ at various potentials. At OCP, the I_Ψ and I_δ of the base metal is approximately 22.17% and 30.38%, respectively. As the applied potential decreases to -850 mV, the I_Ψ and I_δ decreases to 12.89% and 13.01%, respectively; with the continued decrease in potential, the I_Ψ and I_δ rapidly increase. The phenomenon is considered to be related to the effect of the cathodic potential on the anodic dissolution and HE behaviour. The steels with the different heat treatments exhibit high I_Ψ and I_δ, and the microstructures after cooling in water exhibit the highest I_Ψ at -850 mV and -1050 mV. It can be concluded that heat treatment facilitates the SCC susceptibilities of steels under various potentials in artificial seawater.

3.3. Surface morphologies after SSRT tests

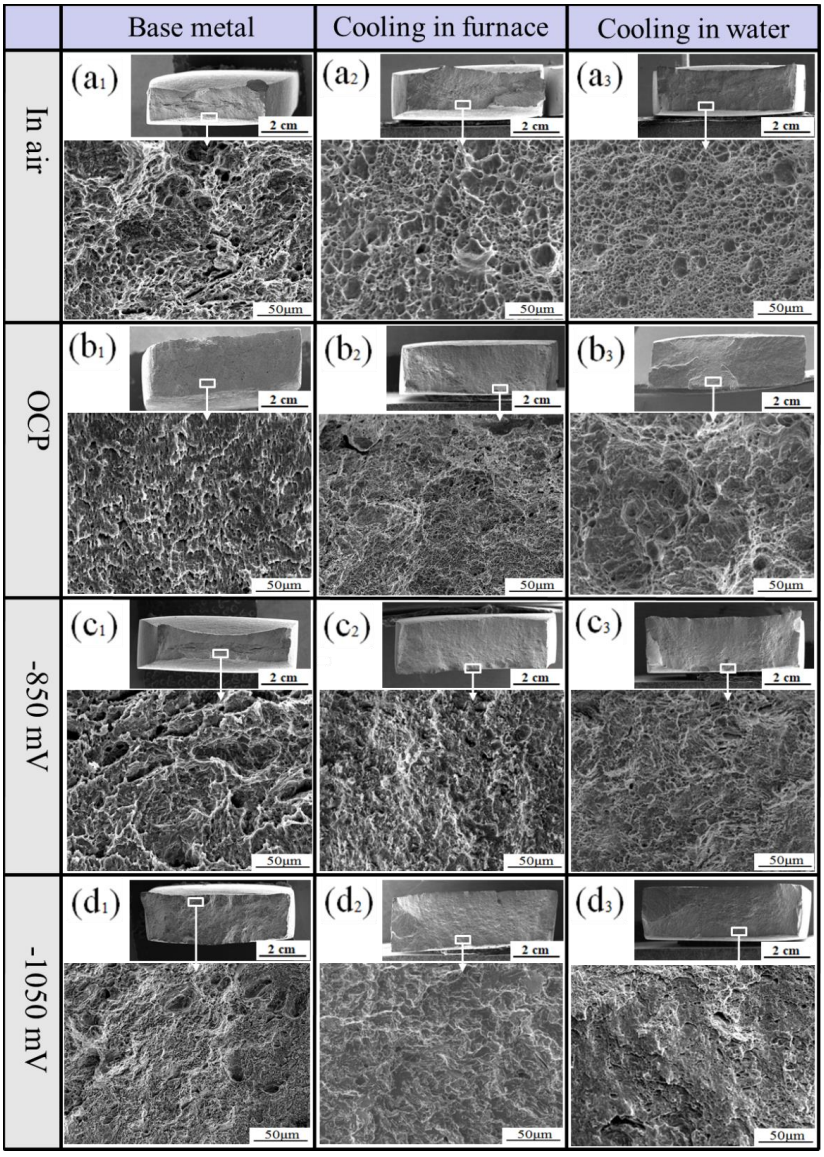

Figure 4. SSRT fracture surfaces of E690 steels with different heat treatments in air and artificial seawater with various potentials.

To further investigate the SCC behaviour, the SSRT fracture surfaces of E690 steel with different heat treatments under various potentials were observed, with the results shown in Fig. 4.

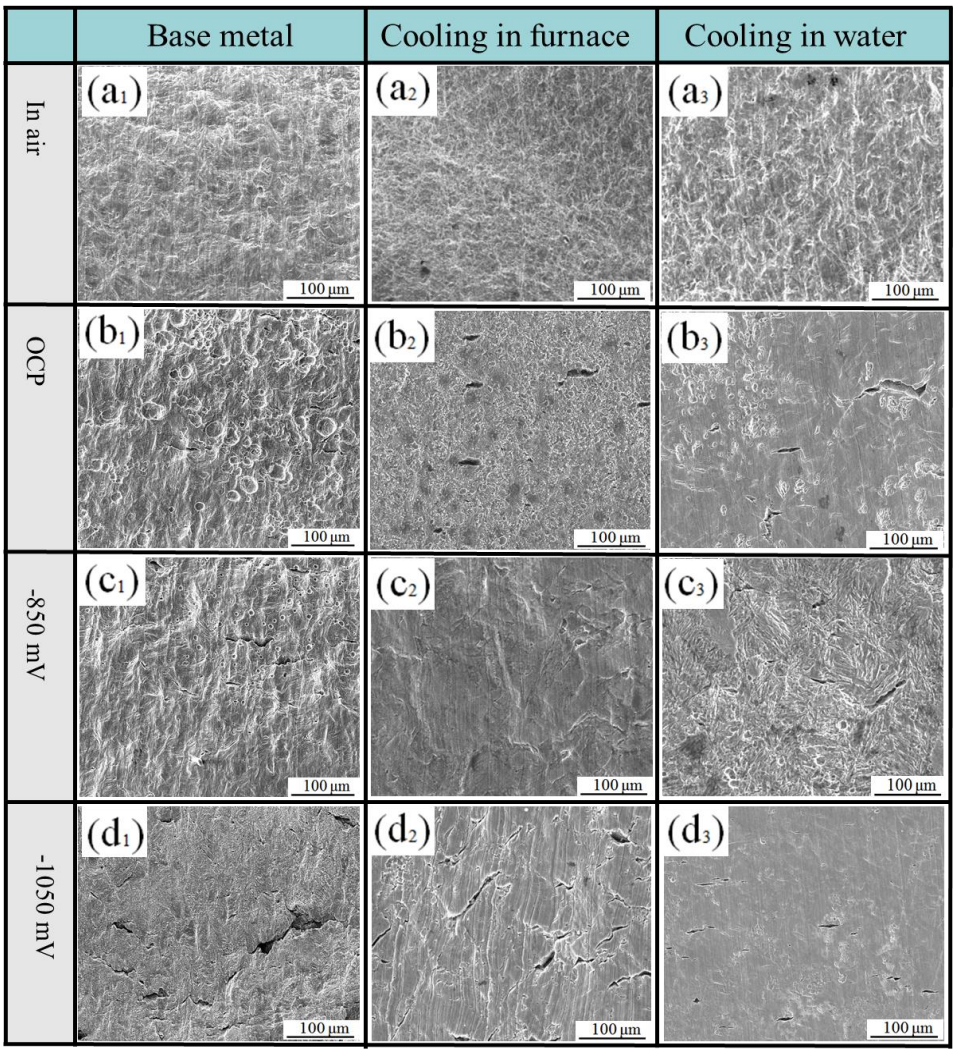

Figure 5. Side faces after SSRT fracture of the E690 steels with different heat treatments in air and artificial seawater at various potentials.

In air (Fig. 4a_1, a_2. a_3), the obvious necking is observed on the steels with different heat treatment, and many dimples occur on the fracture surface, which means the ductile fracture. At OCP (Fig. 4b_1, b_2. b_3), the necking phenomenon recedes for different heat treatments, and the side of the fracture surface becomes smooth comparing to those in air, which is related to the anodic dissolution occurring in artificial seawater. At -850 mV (Fig. 4 c_1, c_2. c_3), the base metal exhibits obvious necking, however, the necking phenomenon do not happen on the fractures of the steels with cooling in furnace and water; the dimples only occur on the fracture of the base metal, the side of the fractures surface on the steels after tempering exhibit quasi-cleavage fracture, which is related HE. With negatively continued decreasing potential to -1050 mV (Fig. 4 d_1, d_2. d_3), no necking phenomenon is observed on the fracture of the steels, and the brittle fracture occurs.

Fig. 5 shows the side faces after SSRT fracture of the steels with different heat treatments under

various potentials in artificial seawater. In air (Fig. 4a_1, a_2, a_3), comparing the surfaces of the steels after tempering, the surface of the base metal obviously exhibits deformation, which is related to the strengthening process. At OCP (Fig. 5b_1, b_2, b_3), serious pitting occurs with some small cracks on the side face of the base metal; uniform corrosion with some relatively wide cracks can be observed on the surface of the steel after cooling in a furnace. Moreover, some relatively slight pits and long cracks appear on the surface of the steel after cooling in water. At -850 mV (Fig. 5c_1, c_2, c_3), the pits and uniform corrosion are inhibited to a certain degree, and some fine cracks appear on the surfaces. At -1050 mV (Fig. 5d_1, d_2. d_3), pitting is absolutely inhibited, and the number of cracks decreases with an increasing cooling rate during the tempering process.

3.4. Electrochemical behaviour

Fig. 6 shows the polarization curves of E690 steels with different heat treatments and their corresponding corrosion currents and corrosion potentials in artificial seawater. In Fig. 6a, the polarization curves show that the electrochemical reaction is controlled by the cathodic reaction. After tempering, the section of the polarization curves in the cathodic reaction moves to the right, meaning that the cathodic reaction is accelerated. At the same time, the active section of the anodic reaction moves to the left. The polarization curves are fitted, with the results shown in Fig. 6b. The corrosion current densities of the steels after cooling in a furnace and in water indicate that the tempering heat treatment facilitates the corrosion rate. The steels after tempering exhibit a high corrosion potential, meaning that the electrochemical reaction behaviour is influenced by the tempering process.

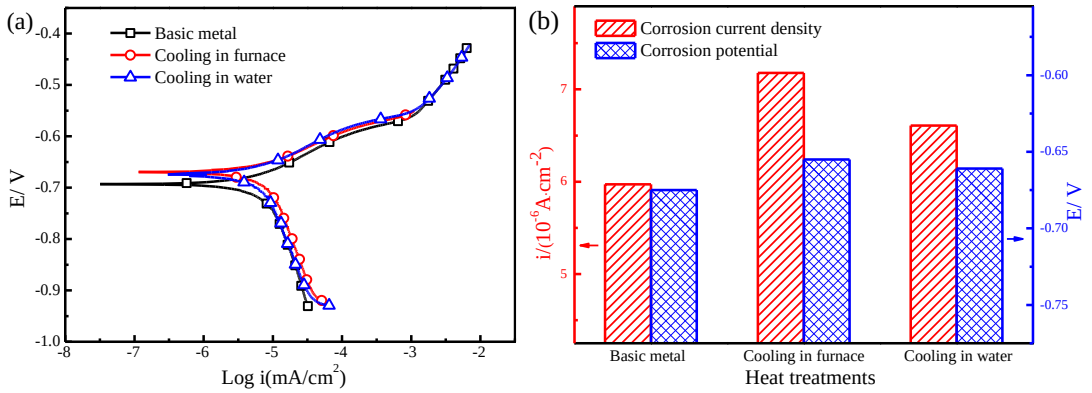

Figure 6. (a) Polarization curves of E690 steels with different heat treatments and (b) corresponding corrosion currents and corrosion potentials in artificial seawater

3.5. Effect of the different treatments on the SCC mechanism of E690 steel

In artificial seawater with a near-neutral pH, the main electrochemical reaction is the oxidation reaction of metal atoms and the oxygen reduction reaction, which can be written as follows:

$$Fe + 2H_2O \leftrightarrow Fe(OH)_2 + 2H^+ + 2e \quad (3)$$

$$2H_2O + O_2 + 4e \leftrightarrow 4HO^- \quad (4)$$

In this work, the electrochemical reaction rate is mainly influenced by the anodic reaction (Fig.

6). The rate of anodic dissolution is affected by the microstructure, composition, inclusion, dislocation, microresidual stress and other factors in the metal [38-42]. Previous studies have demonstrated that microgalvanic corrosion occurs between the different microstructures, the inclusions and base metal, the grain boundaries and the inside of grain, the precipitated phase and base metal; furthermore, different microresidual stress values and other factors will facilitate the corrosion rate. In this study, after cooling in a furnace, martensite and pearlite and lath bainite form a microgalvanic current, resulting in a high corrosion rate, as shown in Fig. 6. It is demonstrated that a rapid cooling rate will enhance the microresidual stress, which will further accelerate the electrochemical reaction rate[43, 44].

The SCC behaviour was considered to be related to the anodic dissolution in the near-neutral pH environment where the cracks were initiated [45]. Anodic dissolution usually occurs inside the grain, with the grain boundaries working as cathodic electrodes during the electrochemical reaction process. The stress tends to concentrate around the pits resulting from local corrosion under the stress field, which further leads to the initiation of cracks [46]. As shown in Fig. 5, many micropits and cracks appear on the steel surface. The anodic dissolution reaction occurs inside the grain in a near-neutral pH environment, which will induce the initiation of a crack. The concentration of stress around the crack tip and the pits will further facilitate the anodic dissolution reaction rate. In the crack initiation stage, the SCC behaviour is affected by the anodic reaction. Thus, when comparing the fracture surface in air (Fig. 4a_1, a_2, a_3), a flat surface appears on the fracture surface at the OCP (Fig. 4b_1, b_2, b_3). The phenomenon is related to the occurrence of anodic dissolution during crack propagation. The anodic dissolution enhances the propagation of the crack in the shallow crack stage. In this work, the high corrosion rates of the steels after tempering result in high SCC susceptibilities (I_ψ) compared to that of the base metal, as shown in Fig. 3. Under the stress field, the stress tends to concentrate at the location between the different microstructures because of their different hardness and elongation. The concentration of the stress will accelerate the corrosion rate and enhance the propagation of the crack, which further increases the susceptibility. As shown in Figs. 1 and 3a, the steel after cooling in a furnace exhibits the highest SCC susceptibilities because of the existence of martensite and pearlite among the lath bainite at the OCP.

When the cathodic potential decreases to -850 mV, the anodic reaction is inhibited, which slows the electrochemical reaction [5]. As shown in Figs. 5c_1, c_2 and c_3, the pitting and uniform corrosion on the side surfaces of the fractures are relatively inhibited. This will further inhibit the initiation of the cracks and the propagation of the shallow cracks, resulting in an influence on the SCC susceptibility. Thus, at -850 mV, the SCC susceptibility of the base metal decreases. However, steels with tempering show increased SCC susceptibilities. Moreover, the fracture surface of the base metal shows ductile fracture characteristics, and the fracture surfaces of the steels after tempering exhibit brittle fracture. This indicates that the base metal and the steels after tempering show different SCC mechanisms. A previous study demonstrated that the electrochemical potential of the hydrogen evolution reaction is approximately -720 mV (vs. SCE), suggesting that hydrogen atoms are produced from the hydrogen evolution reaction. It has been stated that steel will exhibit hydrogen-induced plasticity with a certain amount of hydrogen atoms, which then decreases the SCC susceptibility [9]. A recent study indicated that heat treatment would enhance the concentration of dislocations, resulting in different microstructures and further accelerating HE susceptibility. Thus, the steels after tempering show high

SCC susceptibility.

With the cathodic potential decreasing to -1050 mV, the electrochemical corrosion on the steel surface is almost completely inhibited (Fig. 5d_1, d_2, d_3). The SCC behaviour is controlled by the HE mechanism at a relatively negative cathodic potential, and the HE susceptibility increases with a decreasing cathodic potential when the hydrogen content in the metal exceeds the threshold value. Thus, as the cathodic potential decreases to -1050 mV, the SCC susceptibilities of the steels increase with brittle fracture characteristics on the fracture surfaces (Fig. 4d_1, d_2, d_3). In this work, because of the assistance of a large number of dislocations and the martensite and pearlite resulting from the heat treatment, the steels after tempering show a higher SCC susceptibility than the base metal.

4. CONCLUSIONS

The SCC behaviour and mechanism of E690 steel in artificial seawater is mainly controlled by anodic dissolution at the OCP. The steels after tempering show high corrosion current densities, which further leads to high SCC susceptibilities at the OCP. Because of the interaction effect of martensite, pearlite and lath bainite, the steel after cooling in a furnace shows the highest SCC susceptibility.

With a gradually decreasing cathodic potential, the steels with different heat treatments show different variation tendencies. As the cathodic potential decreases to -850 mV, the anodic reaction is inhibited, resulting in a decrease in the SCC susceptibility of the base metal; however, the SCC susceptibilities of the steels after tempering increase, resulting from the promotion of HE at a relatively negative cathodic potential. At -1050 mV, the SCC susceptibilities of the steels with different heat treatments increase due to the further promotion of HE. The SCC susceptibilities of the steels after tempering are higher than that of the base metal at various potentials. The above phenomenon is related to the higher HE susceptibilities of the steels after tempering compared to that of the base metal.

ACKNOWLEDGEMENT
The authors gratefully acknowledge financial support of Yuli Materials Corrosion National Observation and Research Station and Wuhan Materials Corrosion National Observation and Research Station.

References

1. X. Li, D. Zhang, Z. Liu, Z. Li, C. Du, C. Dong, *Nature*, 527 (2015) 441.
2. H. Qian, D. Xu, C. Du, D. Zhang, X. Li, L. Huang, L. Deng, Y. Tu, J.M.C. Mol, H.A. Terryn, *J. Mater. Chem.* A, 2017, 5(5): 2355-2364.
3. H. Yao, D. Leping, J. Pengfei, H. Luyao, Q. Hongchang, Z. Dawei, L. Xiaogang, T.H. A., *ACS Appl. Mater. Interfaces*, 2018, 10(27) 23369-23379.
4. D. Zhang, L. Wang, H. Qian, X. Li, *J. Coat. Technol. Res*., 2016, 13(1) 11-29.
5. Y. Li, Z. Liu, E. Fan, Y. Huang, Y. Fan, B. Zhao, *J. Mater. Sci. Technol*., 2019.
6. Z. Liu, X. Li, Y. Cheng, *J. Mater. Eng. Perform*., 20 (2011) 1242-1246.
7. Z. Liu, X. Li, Y. Cheng, *Corros. Sci*., 55 (2012) 54-60.
8. H. Ma, Z. Liu, C. Du, H. Wang, C. Li, X. Li, *Mater. Sci. Eng.* A, 642 (2015) 22-31.
9. Z. Liu, X. Wang, C. Du, J. Li, X. Li, *Mater. Sci. Eng*. A, 658 (2016) 348-354.

10. Y. Prawoto, A. Moin, M. Tadjuddin, W.W. Nik, *Eng. Fail. Anal*., 18 (2011) 1858-1866.
11. D. Hejazi, A. Haq, N. Yazdipour, D. Dunne, A. Calka, F. Barbaro, E. Pereloma, *Mater. Sci. Eng*. A, 551 (2012) 40-49.
12. BEIDOKHTI, DOLATI, KOUKABI, H. A., *Mater. Sci. Eng*. A, 507 (2009) 167-173.
13. D. Lopez, W. Schreiner, S. De Sanchez, S. Simison, *Appl. Surf. Sci.*, 236 (2004) 77-97.
14. D. Lopez, W. Schreiner, S. De S¨¢nchez, S. Simison, *Appl. Surf. Sci*. 207 (2003) 69-85.
15. J. Bulger, B. Lu, J. Luo, *J. Mater. Sci*., 41 (2006) 5001-5005.
16. J. wiek, *J. Mater. Process. Technol*., 164 (2005) 1007-1013.
17. M. Li, Y. Cheng, *Electrochim. Acta*, 53 (2008) 2831-2836.
18. Y. Cheng, L. Niu, *Electrochem. Commun*., 9 (2007) 558-562.
19. Z. Liu, X. Li, C. Du, L. Lu, Y. Zhang, Y. Cheng, *Corros. Sci.*, 51 (2009) 895-900.
20. Z. Liu, X. Li, C. Du, G. Zhai, Y. Cheng, *Corros. Sci.*, 50 (2008) 2251-2257.
21. Y. Li, *Int. J. Electrochem. Sci*., 11 (2016) 5021-5034.
22. Y. Li, W. Wu, Z. Liu, X. Li, J. Zhao, *Corros. Sci.*, (2019) 108336.
23. B. Fang, A. Atrens, J. Wang, E.-H. Han, Z. Zhu, W. Ke, *J. Mater. Sci*., 38 (2003) 127-132.
24. M. Li, Y. Cheng, Mechanistic investigation of hydrogen-enhanced anodic dissolution of X-70 pipe steel and its implication on near-neutral pH SCC of pipelines, *Electrochim. Acta*, 52 (2007) 8111-8117.
25. T. Zhao, Z. Liu, C. Du, C. Dai, X. Li, B. Zhang, *Mater. Sci. Eng*. A, 708 (2017) 181-192.
26. T. Zhao, Z. Liu, C. Du, C. Liu, X. Xu, X. Li, *Corros. Sci*., 142 (2018) 277-283.
27. Z. Liu, W. Hao, W. Wu, H. Luo, X. Li, *Corros. Sci*., 148 (2019) 388-396.
28. Z. Liu, X. Li, Y. Cheng, *Electrochim. Acta*, 60 (2012) 259-263.
29. H. Tian, X. Wang, Z. Cui, Q. Lu, L. Wang, L. Lei, Y. Li, D. Zhang, *Corros. Sci*., (2018).
30. H. Tian, J. Xin, Y. Li, X. Wang, Z. Cui, *Corros. Sci.*, 158 (2019) 108089.
31. D.C. Kong, X.Q. Ni, C.F. Dong, X.W. Lei, L. Zhang, C. Man, J.Z. Yao, X.Q. Cheng, X.G. Li, *Mater. Des*., 152 (2018) 88-101.
32. D.C. Kong, X.Q. Ni, C.F. Dong, L. Zhang, C. Man, J.Z. Yao, K. Xiao, X.G. Li, *Electrochim. Acta*, 276 (2018) 293-303.
33. H. Ma, Z. Liu, C. Du, X. Li, Z. Cui, *Mater. Sci. Eng*. A, 650 (2016) 93-101.
34. W. Wu, Z. Liu, X. Li, C. Du, Z. Cui, *Mater. Sci. Eng*. A, 759 (2019) 124-141.
35. J. Hu, L.-X. Du, H. Xie, F.-T. Dong, R. Misra, *Mater. Des*., 60 (2014) 302-309.
36. J. Moon, S.-J. Kim, C. Lee, *Mater. Sci. Eng*. A, 528 (2011) 7658-7662.
37. G.A. Young, N. Lewis, D.S. Morton, The stress corrosion crack growth rate of alloy 600 heat affected zones exposed to high purity water, in: USNRC-ANL Conference on Vessel Head Penetration Inspection, Cracking, and Repairs, 2003.
38. Z.Y. Liu, X.G. Li, Y.F. Cheng, *Electrochim. Acta*, 56 (2011) 4167-4175.
39. Z. Liu, L. Lu, Y. Huang, C. Du, X. Li, *Corrosion*, 70 (2014) 678-685.
40. Z. Cui, Z. Liu, L. Wang, X. Li, C. Du, X. Wang, *Mater. Sci. Eng*. A, 677 (2016) 259-273.
41. L. Wang, Z. Liu, Z. Cui, C. Du, X. Wang, X. Li, *Corros. Sci*., 85 (2014) 401-410.
42. C. Liu, R.I. Revilla, D. Zhang, Z. Liu, A. Lutz, F. Zhang, T. Zhao, H. Ma, X. Li, H. Terryn, *Corros. Sci*., 138(2018) 96-104
43. Y. Li, Z. Pei, B. Zaman, Y. Zhang, H. Yuan, B. Cao, *Mater. Res. Express*, 5 (2018) 116516.
44. Y. Li, L. Song, F. Sun, *Int. J. Electrochem. Sci.*, 13 (2018) 10155-10172.
45. B. Brown, C. Fujii, E.P. Dahlberg, *J. Electrochem. Soc*., 116 (1969) 218-219.
46. B. Harle, J. Beavers, *Corrosion*, 49 (1993) 861-863.